Communication: Imaging the indirect dissociation dynamics of temporary negative ion: N2O− → N2 + O−

Lei Xia, Bin Wu, Hong-Kai Li, Xian-Jin Zeng, and Shan Xi Tian

Articles you may be interested in

First-principles investigation of the dissociation and coupling of methane on small copper clusters: Interplay of collision dynamics and geometric and electronic effects
J. Chem. Phys. **142**, 184308 (2015); 10.1063/1.4919948

Chemistry at molecular junctions: Rotation and dissociation of O2 on the Ag(110) surface induced by a scanning tunneling microscope
J. Chem. Phys. **139**, 074702 (2013); 10.1063/1.4818163

Static surface temperature effects on the dissociation of H2 and D2 on Cu(111)
J. Chem. Phys. **137**, 054703 (2012); 10.1063/1.4738956

Communication: Quasiclassical trajectory calculations of correlated product-state distributions for the dissociation of (H2O)2 and (D2O)2
J. Chem. Phys. **135**, 151102 (2011); 10.1063/1.3655564

Molecular dynamics investigations of the dissociation of Si O 2 on an ab initio potential energy surface obtained using neural network methods
J. Chem. Phys. **124**, 134306 (2006); 10.1063/1.2185638

Communication: Imaging the indirect dissociation dynamics of temporary negative ion: $N_2O^- \rightarrow N_2 + O^-$

Lei Xia, Bin Wu, Hong-Kai Li, Xian-Jin Zeng, and Shan Xi Tian[a)]
Hefei National Laboratory for Physical Sciences at the Microscale and Department of Chemical Physics, University of Science and Technology of China, 96 Jinzhai Road, Hefei, Anhui 230026, China

We reported an imaging study of the dissociation dynamics of temporary negative ion N_2O^- formed in the low-energy electron attachment, $e^- + N_2O \rightarrow N_2O^- \rightarrow N_2 + O^-$. With the help of *ab initio* molecular dynamics calculations, the evolution of momentum distributions of the O^- fragment in terms of the electron attachment energy is identified as the result of a competition between two distinctly different indirect pathways, namely, climbing over and bypassing the energy ridge after the molecular structure bending. These two pathways prefer leaving the N_2 fragment at the high vibrational and rotational states, respectively. © *2012 American Institute of Physics.*
[http://dx.doi.org/10.1063/1.4760278]

Unimolecular dissociation provides a suitable vessel for investigation of chemical reaction dynamics.[1] Direct and indirect processes represent the two major classes of the molecular dissociation induced by photoabsorption or collision. In the direct case, the fragmentation proceeds too fast to develop internal energy of the target molecule; in the indirect case, the dissociation usually experiences a metastable state which has a sufficiently long time to allow the internal energy redistribution. For the latter, the final state distributions of the fragments no longer reflect the initial state wavefunction like they do in the direct dissociation. The details of the indirect dissociation are, even in a black box, rather difficult to be revealed, unless the final states of all fragments can be measured precisely and the various dissociation pathways on the potential energy surface (PES) at the intermediate state can be theoretically simulated.[2] Electron-molecule resonance, also know as temporary negative ion (TNI), is a typical intermediate resonant state formed in the low-energy electron attachment to molecule and may decay via dissociation to a negatively charged ion and one or more neutral fragments.[3] Due to the very short lifetime of TNI (from microseconds to femtoseconds or less, depending on the resonance types[3]), most dissociations, even for the large flexible molecules, are believed to be the direct processes.[4–6] Here we present an imaging study of the dissociation dynamics of a triatomic TNI N_2O^-, $N_2O^- \rightarrow N_2 + O^-$, by the angular-resolved detection of the O^- fragment. Two modes of the O^- momentum distributions confidently provide an evidence of the indirect dissociation: after the structural bending of the linear molecule, two distinctly different dissociation pathways, namely, climbing over and bypassing the energy ridge on the PES of N_2O^-, compete with each other.

The full-collision dynamic picture of the dissociative electron attachment (DEA) via the predissociation-state TNI, especially for a polyatomic molecular target, is still a chal-lenge both in the experiments and theoretical calculations.[5] In the low-energy (less than several eV) electron attachment to N_2O, several series of vibrational excitations of N-O bond stretching (υ_1), N-N-O bond bending (υ_2), and N-N bond stretching (υ_3) modes were observed around the N_2O^- $^2\Pi$ shape resonant state;[7,8] a diffuse band including two peaks (0.7 eV and 2.4 eV) in the O^- yield spectra of the DEA process[7,9] can also be attributed to this resonant state on the basis of the recent theoretical calculations.[10] However, a long-term argument about the coexistence of a $^2\Sigma$ resonant state in this energy range arose from the measurements of the angular-resolved differential cross sections of the O^- ion in a limited angular range (30° to 130°).[7,11] It is also puzzling that the kinetic energies of the O^- ion were quite large even at the low electron incident energies.[8] Herein, these misconceptions will be clarified.

The O^- momentum distributions for the DEA process of N_2O have been measured at the electron energies of 0.70, 1.90, 2.25, and 2.60 eV by using our newly developed anion velocity image mapping apparatus.[12] As shown in Fig. 1, the time-sliced images of the O^- momentum clearly show the pattern evolution, namely, from the half-rings (Fig. 1(a)) to the tetrad-petal-like images (Figs. 1(c) and 1(d)). Their common features are: the stronger backward scattering, the nodes along the z axis, and the nearly same size of the momentum rings. The ring size is determined by the O^- velocity projected on the x-z detection plane. Before going to reveal the dissociation dynamics underneath these images, the PES of N_2O^- is plotted within the Jacobi coordinates R and γ (see their definitions in the upright panel of Fig. 2) on the basis of the configuration interaction calculations at CASSCF(11,10)/6-311G(d) level (more details can be found in the supplementary material[17]). In the formation of N_2O^- at $^2\Pi$ resonant state, the excess electron is captured and occupies at the lowest unoccupied molecular orbital π^*. Due to the Renner-Teller effect, the $^2\Pi$ resonant state undergoes splitting into $^2A''$ and $^2A'$ states in asymptote if the N-N-O bond bending (υ_2) vibration is involved in the electron attachment. No other

---

a)Author to whom correspondence should be addressed. Electronic mail: sxtian@ustc.edu.cn.
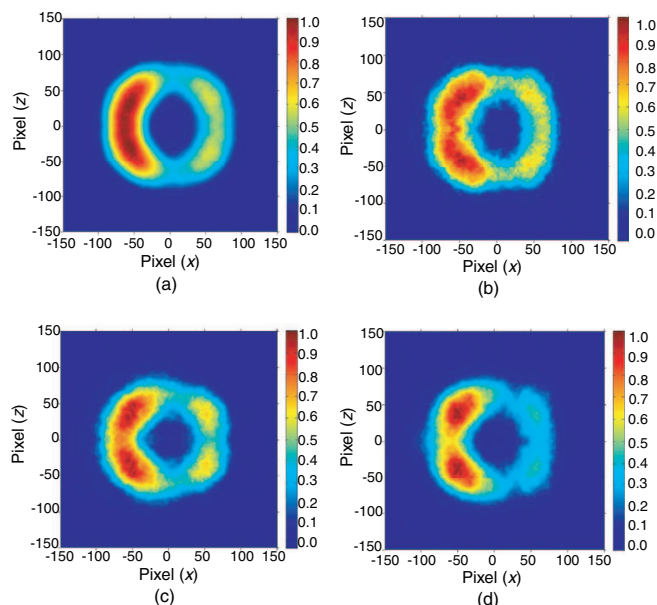
137, 151102-1

FIG. 1. Sliced images of the O^- momentum at the electron attachment energies of 0.70 eV (a), 1.90 eV (b), 2.25 eV (c), and 2.60 eV (d). The electron incident direction is from the left to the right. The anion intensities of the images are normalized, respectively.

states could be involved in the DEA processes investigated here.[8–10] In Fig. 2, the black thick line indicates the PES intersection curve at the $^2\Pi$ resonant state, where the N-O bond stretching (v_1) and N-N bond stretching (v_3) vibrations are permitted (the linear molecular structure is still kept). The direct dissociation $N_2O^- \to N_2 + O^-$ at the $^2\Pi$ resonant state by an elongation of N-O bond may be hindered due to an energy barrier about 0.68 eV (close to the previously speculated value 0.5 eV[9]), but an indirect dissociation is feasible. Af-
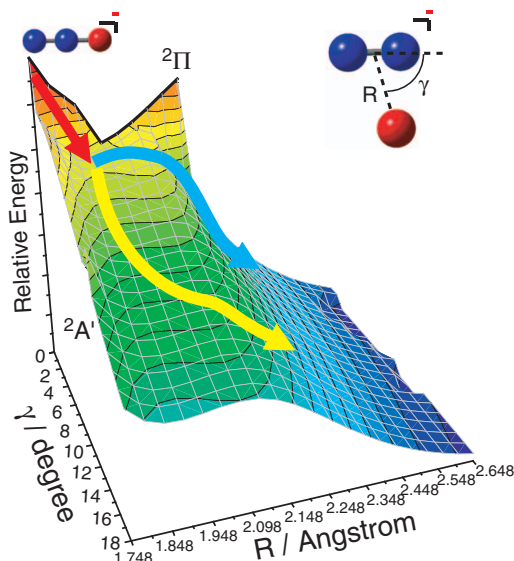

FIG. 2. Potential energy surface in the Jacobi coordinate. The Jacobi coordinate is defined as the upright panel: R is the distance between oxygen and the midpoint of molecular nitrogen bond and γ is the orientation angle of the N_2 bond axis. The red arrow denotes the simultaneous TNI structure bending; The blue and yellow arrows represent the over-the-ridge and the ridge-bypassing, respectively.

ter the vertical attachment, the linear structure (R = 1.748 Å and $\gamma = 0°$) will be slightly bent ($\gamma \approx 2°$) along the red arrow which points the low energy region then is followed with two distinctly different dissociation pathways. One pathway is named as the "over-of-the-ridge" path and labeled with the blue arrow, in which the energy barrier along the R axis needs to be overcome. This energy ridge dramatically collapses with the increase of γ, from 0.68 eV (R = 2.198 Å, $\gamma = 0°$) to 0.08 eV (R = 2.048 Å, $\gamma = 20°$); therefore, the N_2O^- can also go down firstly along the declining slope with the increasing γ values, then happens to go through the much lower ridge at a larger γ value. This is noted as the "ridge-bypassing" path and labeled with the yellow arrow. Although these two paths are on the $^2A'$ PES, the over-of-the-ridge path is approximately of the $^2\Pi$ symmetry because it is nearly parallel to the intersection curve of the $^2\Pi$ PES (thick line in Fig. 2). These two different pathways are crucial to reveal the evolution dynamics observed in the O^- momentum images.

The previous experiments showed the O^- kinetic energies were 0.23 and 0.44 eV at the incident energies 0.612 and 2.5 eV, respectively.[8] The thermodynamic energy threshold 0.21 eV of $N_2O^- \to N_2 + O^-$ was determined as well.[8] If the residual energy after the dissociation is completely transformed to be the translational energies of the fragments, the maximum kinetic energy of the O^-, $E_{max} = (E_{incident} - 0.21)/(1 + 16/28)$, should be 0.31, 1.08, 1.30, and 1.52 eV for the attachment energies 0.70, 1.90, 2.25, and 2.60 eV, respectively. By integration of the image data, the kinetic energy distributions of the O^- fragment are plotted in Fig. 3(a). At the different attachment energies, all kinetic energy profiles show the peaks at about 0.33 eV, in accord with the previous results.[8] However, the kinetic energies around 0.33 eV are much lower than the above predictions, implying that the most residual energies should be transformed to be the internal energies of N_2 fragment.

The angular-resolved differential cross sections of the O^- fragment in the kinetic energy range of 0.15–0.50 eV are depicted as the solid circles in Figs. 3(b)–3(e). For the DEA of diatomic molecules within the axial-recoil approximation, the momentum distribution of the anion fragment is determined by[13]

$$\sigma_{anion}(k, \theta, \varphi) \propto \sum_{|\mu|} \left| \sum_{j=1, l=|\mu|} c_j e^{i\delta_j} Y_{l\mu}(\theta, \zeta) \right|^2 \quad (1)$$

where the impinging electron is described by a series of partial waves of the different angular momentum l ($l \geq |\mu|$) and $Y_{l\mu}$ is the spherical harmonics describing the neutral and TNI states. $|\mu|$ equals to $|\Lambda_f - \Lambda_i|$, representing the difference in the projection of the angular momentum along the internuclear axis for the neutral and TNI. In the formation of a resonant state of TNI, the different influences on each partial wave of the impinging electron by the interaction potential of the target result in the phase lags (δ_j) among these partial waves. In practice, the summation of the finite partial wave terms together with the weight parameter c_j can reproduce the momentum distribution of the anionic fragment for single resonant state.[4,5,11] The present DEA should be beyond the
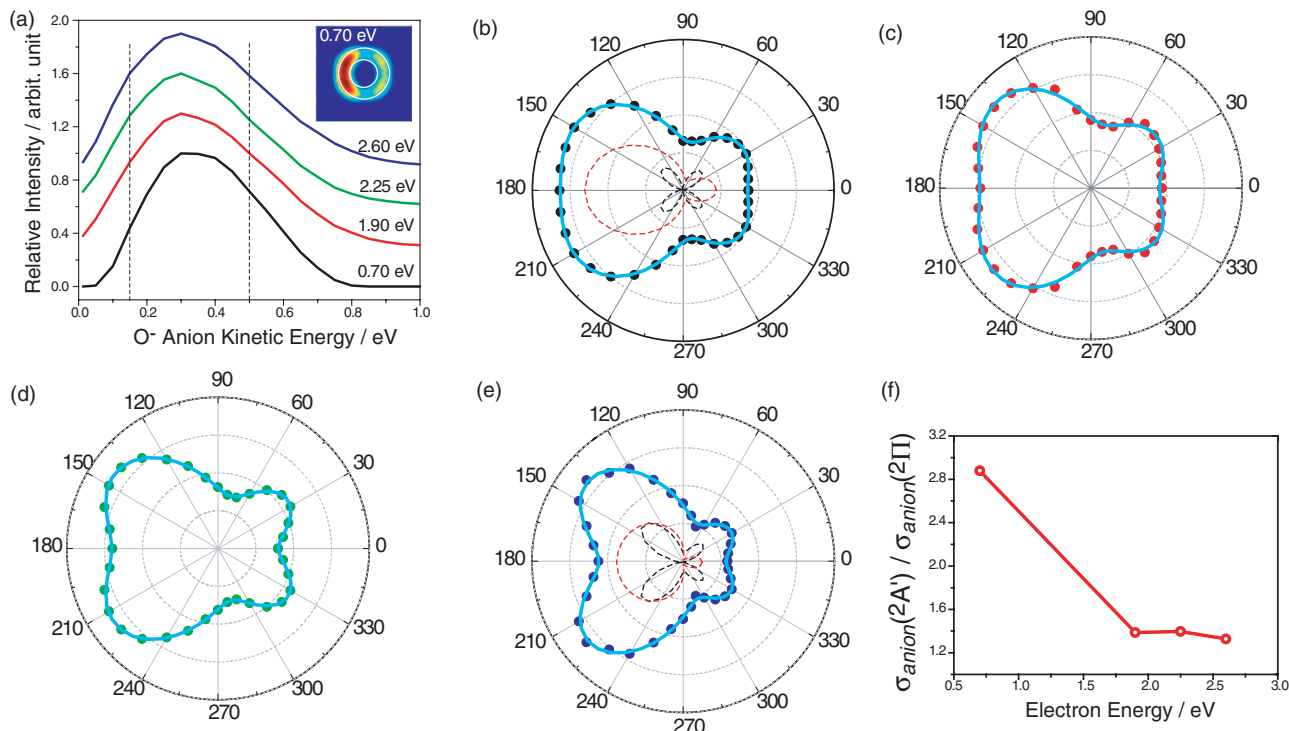
FIG. 3. (a) The kinetic energy distributions of the O$^-$ fragment are plotted by integration of ion signals in the selected annular area of the sliced image in Fig. 1. Two vertical broken lines show the higher intensities in the kinetic energy range of 0.15–0.50 eV which corresponds to the annular area of the sliced image, for example, at the electron incident energy of 0.70 eV, see the inserted panel. The momentum distributions of the O$^-$ fragment in the kinetic energy range of 0.15–0.50 eV at the different electron energies: (b) 0.70 eV, (c) 1.90 eV, (d) 2.25 eV, and (e) 2.60 eV. The broken curves in (b) and (e) represent the momentum distribution via the ridge-bypassing (red) and over-the-ridge (black) dissociation pathways. (f) The branching ratios between the ridge-bypassing [$\sigma_{anion}(^2A')$] and the over-the-ridge [$\sigma_{anion}(^2\Pi)$] pathways.

axial-recoil approximation due to the structural bending ($\gamma \approx 2°$) after the electron attachment. Assuming that the departure between the O$^-$ and N$_2$ fragments is approximately along a new recoil axis, the axial-recoil approximation is supposed to be valid for the dissociation of this slightly bending N$_2$O$^-$. In this binary dissociation, $\Lambda_f = 1$ ($^2\Pi$, the blue arrow) along the over-the-ridge pathway; while $\Lambda_f = 0$ ($^2A'$, the yellow arrow) along the ridge-bypassing pathway. Therefore, the differential cross section of the O$^-$ fragment can be rewritten as

$$\sigma_{anion}(\theta) \propto \left| a_0 Y_{00} + e^{i\delta_1} a_1 Y_{10} + e^{i\delta_2} a_2 Y_{20} \right|^2$$
$$+ \left| b_0 Y_{11} + e^{i\delta_3} b_1 Y_{21} + e^{i\delta_4} b_2 Y_{31} \right|^2, \quad (2)$$

where the over-the-ridge and ridge-bypassing pathways are represented with the first and second terms in the right. As shown in Figs. 3(b)–3(e), the excellent experimental data fittings using Eq. (2) are achieved with the high correlations (>0.99). The fitted parameters (given in the supplementary material) indicate that the predominant scattering amplitudes are $s\Sigma(^2A') + d\Pi$ at the attachment energies of 0.70 and 1.90 eV, while $s\Sigma(^2A') + p\Pi + d\Pi$ at 2.25 and 2.60 eV. The previous argument about using either Σ or Π symmetry in fitting the momentum distribution[7,11] now can be clarified satisfyingly.

To elucidate the different roles of each pathway, the momentum distributions at 0.70 and 2.60 eV are reproduced by using the fitted parameters and shown as the broken curves

in Figs. 3(b) and 3(e). The backward-scattering features are primarily attributed to the ridge-bypassing pathway (the red broken curves), while the over-the-ridge pathway leads to the significant tetrad-petal of the O$^-$ momentum distribution (the black broken curves). In Fig. 3(f), the branching ratio of these two pathways [$\sigma_{anion}(^2A') / \sigma_{anion}(^2\Pi)$] has been plotted by the data integration over θ ($0 \sim 2\pi$) using the fitting parameters. The contribution of the ridge-bypassing pathway [$\sigma_{anion}(^2A')$] overwhelms that of the over-the-ridge pathway [$\sigma_{anion}(^2\Pi)$] at these four attachment energies, although the former decreases quickly from 0.70 eV to 1.90 eV. It is amazing that even at the higher energy 2.60 eV the dissociation N$_2$O$^- \rightarrow$ N$_2$ + O$^-$ still prefers the ridge-bypassing path.

According to the momentum and energy conservation principles and supposing that the most O$^-$ anions have the kinetic energy of 0.33 eV (the central value of the kinetic energy distributions in Fig. 3(a)), the N$_2$ species should carry out the translational energy about 0.19 eV, but have the different internal energies, 0.00, 1.17, 1.52, and 1.87 eV at the attachment energies, 0.70, 1.90, 2.25, and 2.60 eV, respectively. A quite striking question is how these internal energies are participated into, e.g., the high rotational quanta j, vibrational quanta υ, or both of N$_2$? This is definitely dependent on the dissociation paths or the dynamic trajectories on the PES of Fig. 2.

Due to the extremely low cross sections of DEA, the electron monochromator is still unavailable in the present studies.[12] The energy spread of the incident electron is
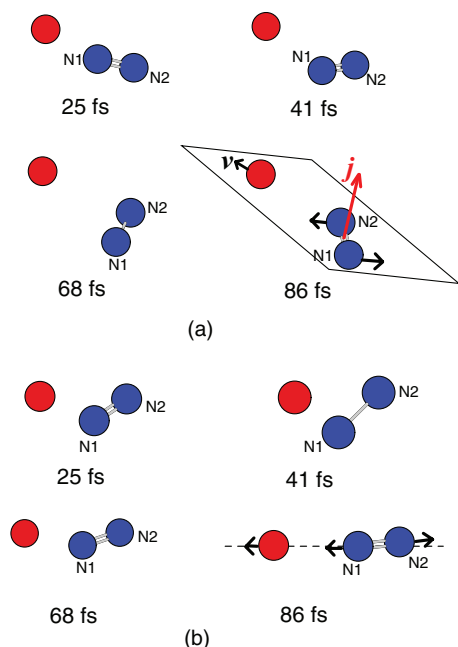
FIG. 4. Eight frames of two sample trajectories with the low initial excess energy of 0.01 eV (a) and the high energy of 1.00 eV (b). Oxygen atom is in red and nitrogen atom is in blue.

±0.3 eV, thereby the possible rovibrational states of N_2 cannot be resolved in the O^- kinetic-energy distribution profiles (see Fig. 3(a)). We performed the *ab initio* molecular dynamics simulations for the dissociation trajectories of the N_2O^- by using the atom-centered density matrix propagation method [ADMP-B3LYP/6-311G(d), more details can be found in the supplementary material]. As mentioned above, the structural propagation is initiated in the Franck-Condon region for the vertical attachment to the linear N_2O. Quasi-classical trajectories starting with two typical initial internal energies 0.01 and 1.00 eV of the TNI can mimic two different DEA processes at the lowest and highest attachment energies. The snapshots of the sample trajectories are selected as eight frames of Fig. 4. At 20 fs, the N_2O^- structure is slightly bent [angle (O-N-N) is about $177°$] and the N-O bond breaks. For the low internal energy, see Fig. 4(a), N_2 fragment further receives the torque from the N-N-O bond bending. A vector correlation $v \perp j$ is observed, where v is the O^- velocity and j is the rotational moment of N_2 (potentially at the higher rotational quanta). For the high internal energy, see Fig. 4(b), the vibrational excited N_2 fragment is observed. At 86 fs, N_2 and O^- fragments are almost aligned. It is noted that there are still some trajectories exhibiting the highly rotating N_2, which is similar to the scenario of the low internal energy simulations. This is in line with our conjecture that the N_2 species would like to continuously receive the torque by the molecular bending due to the large PES gradient along the γ axis. Therefore, the ridge-bypassing pathway is still predominant even at the higher energies (see Fig. 3(f)). The quasi-classical trajectories provide very good qualitative descriptions to the significant differences of these two dissociation pathways. For example, at the incident energy of 1.90 eV, the rotational quanta of N_2 could reach $j \approx 68$ [$E_{int} = j(j+1)h^2/8\pi^2 I$, where the total internal energy $E_{int} = 1.17$ eV, I is the moment of inertia of N_2]

at the vibrational ground state $v = 0$, if the dissociation occurs along the ridge-bypassing pathway; or the N_2 fragment may be at the vibrational excited state $v \approx 4$ without the rotational excitation, if the dissociation proceeds in the over-the-ridge pathway. In a recent theoretical study, the authors also suggested that the strong rotation-exited N_2 fragment could be produced together with O^- ion on the $^2A'$ PES while the dissociation was inhibited on the $^2A''$ PES.[14] Herein, the vibration-excited N_2 fragment as the minor is proposed to be produced via the over-the-ridge path on the $^2A'$ PES.

In summary, we reported the convincing experimental evidence about the complicated indirect dissociation dynamics of N_2O^-. The product state distribution is heavily related to the state evolution of N_2O^-, rather than the neutral state. The present electronic structure calculations and dynamics simulations can provide us for a good qualitative picture of the indirect dissociations, but the competition with electron autodetachment due to the coupling with the electron continuum[15] is ignored. The more sophisticated quantum scattering calculations should be required for the dissociation dynamics of TNI.[15,16] The previous work using anion mass spectrometer proposed that some unanticipated products could be produced via the indirect process of DEA.[16] The present anion velocity imaging spectrometry is a much more promising reaction microscope providing insights into the complicated dynamics of the DEA processes.

[1] T. Bear and W. L. Hase, *Unimolecular Reaction Dynamics: Theory and Experiment* (Oxford University Press, Oxford, 1996).

[2] R. Schinke, *Photodissociation Dynamics* (Cambridge University Press, Cambridge, 1993).

[3] L. G. Christophorou, D. L. McCorkle, and A. A. Christodoulides, in *Electron-Molecule Interactions and Their Applications*, edited by L. G. Christophorou (Academic, New York, 1984), Vol. 1.

[4] B. Wu, L. Xia, Y.-F. Wang, H.-K. Li, X.-J. Zeng, and S. X. Tian, Phys. Rev. A **85**, 052709 (2012).

[5] H. Adaniya, B. Rudek, T. Osipov, D. J. Haxton, T. Weber, T. N. Rescigno, C. W. McCurdy, and A. Belkacem, Phys. Rev. Lett. **103**, 233201 (2009); **106**, 049302 (2011); N. Bhargava Ram, V. S. Prabhudesai, and E. Krishnakumar, *ibid.* **106**, 049301 (2011).

[6] C. König, J. Kopyra, I. Bald, and E. Illenberger, Phys. Rev. Lett. **97**, 018105 (2006).

[7] L. Andrić and R. I. Hall, J. Phys. B **17**, 2713 (1984).

[8] M. Allan and T. Skalický, J. Phys. B **36**, 3397 (2003).

[9] R. D. Rempt, Phys. Rev. Lett. **20**, 1337 (1968); F. Brüning, S. Matejcik, E. Illenberger, Y. Chu, G. Senn, D. Muigg, G. Denifl, and T. D. Märk, Chem. Phys. Lett. **292**, 177 (1998); P. J. Chantry, J. Chem. Phys. **51**, 3369 (1969).

[10] L. A. Morgan, C. J. Gillan, J. Tennyson, and X. Chen, J. Phys. B **30**, 4087 (1997); M. H. F. Bettega, C. Winstead, and V. McKoy, Phys. Rev. A **74**, 022711 (2006).

[11] M. Tronc, F. Fiquet-Fayard, C. Schermann, and R. I. Hall, J. Phys. B **10**, L459 (1977).

[12] B. Wu, L. Xia, H.-K. Li, X.-J. Zeng, and S. X. Tian, Rev. Sci. Instrum. **83**, 013108 (2012).

[13] T. F. O'Malley and H. S. Taylor, Phys. Rev. **176**, 207 (1968).

[14] H. U. Suter and T. Greber, J. Phys. Chem. B **108**, 14511 (2004).

[15] J. R. Taylor, *Scattering Theory: The Quantum Theory of Nonrelativistic Collisions* (Wiley, New York, 1972).

[16] W.-Y. Wang, S. X. Tian, and J. L. Yang, Phys. Chem. Chem. Phys. **13**, 15597 (2011); H. Abdoul-Carime, S. Gohlke, and E. Illenberger, *ibid.* **6**, 161 (2004).

[17] See supplementary material at http://dx.doi.org/10.1063/1.4760278 for the experimental and theoretical methods, and the fitted parameters.